Shear Wave Velocity- and Geology-Based Seismic Microzonation of Port-au-Prince, Haiti

Brady R. Cox,[a] **M.EERI, Jeff Bachhuber,**[b] **M.EERI,**
Ellen Rathje,[c] **M.EERI, Clinton M. Wood,**[a] **M.EERI,**
Ranon Dulberg,[b] **M.EERI, Albert Kottke,**[d] **M.EERI,**
Russell A. Green,[e] **M.EERI, and Scott M. Olson,**[f] **M.EERI**

A seismic site classification microzonation for the city of Port-au-Prince is presented herein. The microzonation is based on 35 shear wave velocity (V_S) profiles collected throughout the city and a new geologic map of the region. The V_S profiles were obtained using the multichannel analysis of surface waves (MASW) method, while the geologic map was developed from a combination of field mapping and geomorphic interpretation of a digital elevation model (DEM). Relationships between mean shear wave velocity over the upper 30 m of the subsurface (V_{S30}) and surficial geologic unit have been developed, permitting code-based seismic site classification throughout the city. A site classification map for the National Earthquake Hazards Reduction Program/International Building Code (NEHRP/IBC) classification scheme is provided herein. Much of the city is founded on deposits that classify as either NEHRP Site Class C or D, based on V_{S30}. Areas of the city requiring additional subsurface information for accurate site classification are noted. [DOI: 10.1193/1.3630226]

INTRODUCTION

On 12 January 2010 a M_w 7.0 earthquake struck the Port-au-Prince region of Haiti. The earthquake was devastating, resulting in an estimated 300,000 or more fatalities. Damage was pervasive and crossed all socioeconomic boundaries, as evidenced by the collapse of homes, schools, hospitals, and government facilities ranging from the Presidential Palace to *bidonvilles* (shanty towns). The enormous death toll was primarily the result of poor building practices, which were unregulated and not in accord with modern seismic building codes. If the city of Port-au-Prince and the other areas of Haiti affected by the earthquake are to be rebuilt in an appropriate manner, the new construction must be based on seismic

[a] University of Arkansas, Department of Civil Engineering, Fayetteville, AR 72701, brcox@uark.edu
[b] Fugro/William Lettis & Associates, Walnut Creek, CA 94596
[c] University of Texas at Austin, Department of Civil, Architectural and Environmental Engineering, Austin, TX 78712
[d] Pacific Earthquake Engineering Center, University of California, Berkeley, CA 94720
[e] Virginia Tech, Department of Civil and Environmental Engineering, Blacksburg, VA 24061
[f] University of Illinois at Urbana-Champaign, Department of Civil and Environmental Engineering, Urbana, IL 61801

Earthquake Spectra, Volume 27, No. S1, pages S67–S92, October 2011; © 2011, Earthquake Engineering Research Institute

standards such as those found in the International Building Code (IBC; ICC 2009) or Eurocode 8 (CEN 2004).

One key step required by seismic provisions in modern building codes is the determination of seismic site classification, which is necessary to determine the expected seismic design forces for the structure. Code-based seismic site classification is based on the subsurface characteristics (soil/rock stiffness, layering, etc.) of the site within the top 30 m. This information is used to group sites into one of several generalized categories that range from "hard rock" to "soft soil" conditions. The National Earthquake Hazards Reduction Program (NEHRP) seismic site classification scheme (BSSC 2003) used in the IBC (ICC 2009) is provided in Table 1. Site Classes A through E are defined primarily based on the mean shear wave velocity in the upper 30 m of the subsurface (V_{S30}), while additional soil properties (i.e., plasticity index, undrained shear strength, etc.) are considered to classify sites that may consist of liquefiable soils or soft clay deposits. It is also possible, although not encouraged, to determine the site class of soil sites based on mean values of the standard penetration test blow count (N_{30}) or undrained shear strength (S_{U30}) in the upper 30 m of the subsurface if shear wave velocity measurements are not available. Determining the site classification is necessary to establish the code-based site response coefficients that control the relative amplitude and shape of the design acceleration response spectrum for the structure.

It is widely recognized that site classification based exclusively on V_{S30} is overly simplified in many circumstances due to factors such as topographic and basin effects, site resonances, sharp impedance contrasts, and deeper structure that influence local ground shaking (Assimaki et al. 2008, Barani et al. 2008, Benjumea et al. 2008, Gallipoli and Mucciarelli 2009, Cassidy and Mucciarelli 2010, Sandikkaya et al. 2010). While several other site classification schemes have been proposed to address these issues (e.g., Rodriguez-Marek et al. 2001, Seed et al. 2001, Zaré and Bard 2002, Park and Hashash 2005, Sun et al. 2005, Phung et al. 2006, Cadet et al. 2008), to date they have not been adopted by building

Table 1. National Earthquake Hazards Reduction Program (NEHRP) seismic site class definitions (BSSC 2003) used in the International Building Code (IBC) (ICC 2009) (converted to metric units and formatted after Sandikkaya et al. 2010)

Site class	V_{S30} (m/s)	N_{30}	S_{U30} (kPa)
A	$V_{S30} > 1{,}500$	-	-
B	$760 < V_{S30} \leq 1{,}500$	-	-
C	$360 < V_{S30} \leq 760$	$50 < N_{30}$	$100 < S_{U30}$
D	$180 \leq V_{S30} \leq 360$	$15 \leq N_{30} \leq 50$	$50 \leq S_{U30} \leq 100$
E	$V_{S30} < 180$	$N_{30} < 15$	$S_{U30} < 50$
	Any profile with more than 3 m of soft clay defined as soil with $PI > 20$, $w \geq 40\%$, and $S_U < 25$ kPa		
F	Soil vulnerable to potential failure or collapse under seismic loading such as liquefiable soils, quick and highly sensitive clays, and collapsible weakly cemented soils		
	Peats and/or highly organic clays (3 m or thicker layer)		
	Very high plasticity clays (8 m or thicker layer with PI > 75)		
	Very thick soft/medium stiff clays (36 m or thicker layer)		

codes and the current standard for code-based design relies on seismic site classification via V_{S30}.

This article presents a seismic site classification microzonation for the city of Port-au-Prince, Haiti. This microzonation effort is based on 35 shear wave velocity (V_S) profiles collected throughout the city and a newly developed geologic map of the region. The V_S profiles were obtained using the multichannel analysis of surface waves (MASW) method, while the geologic map was developed from field reconnaissance mapping and geomorphic interpretation of a 10-m (spatial resolution) digital elevation model (DEM). Relationships between V_{S30} and surficial geologic unit have been developed, allowing V_{S30} to be estimated from geologic information in areas where shear wave velocity measurements were not made. Based on these relationships, the authors developed a NEHRP/IBC-based site classification map for Port-au-Prince. This microzonation map is a preliminary effort that was primarily developed using measurements and observations made during one week of field work. Additional V_S measurements, further geologic mapping, and other information such as fundamental site period will allow this work to be refined in the future. Nonetheless, this initial microzonation map is a critical step in facilitating code-based site classification and seismic design throughout Port-au-Prince as the rebuilding process begins.

GEOLOGY OF PORT-AU-PRINCE

Immediately following the 12 January 2010 Haiti earthquake, the Geotechnical Extreme Events Reconnaissance (GEER) organization, which is funded by the U.S. National Science Foundation (NSF), deployed a team to document the geotechnical and geological aspects of the earthquake (Rathje et al. 2010). Many of the authors of this paper participated in that reconnaissance and soon realized that little detailed geologic information was available for the Port-au-Prince region. The GEER team was able to locate only one small-scale (1:250,000) published geologic map for the entire country of Haiti (Figure 1, Lambert et al. 1987). This map indicates that nearly all of greater Port-au-Prince is founded on three broad geologic units (from youngest to oldest): (1) Quaternary deposits (Qa, not differentiated into Holocene or Pleistocene), (2) Pliocene fan deposits (P), and (3) Miocene deposits (Ms). However, because the Lambert et al. (1987) map is regional, it lacks detail, particularly with respect to Quaternary geology. As a result, the unit boundaries did not match our field observations of geology and damage patterns, and were not consistent with geologically controlled geomorphic features and topography. The largest discrepancy appeared to be the western extent of the Pliocene fan, which is shown in Figure 1 to extend virtually to the bay. Much of downtown Port-au-Prince, where heavy damage occurred during the earthquake, overlies this map unit. The GEER team anticipated that younger, softer Quaternary deposits actually underlay the downtown district and that these deposits amplified the ground shaking in the area (Rathje et al. 2011). It was clear that any future microzonation efforts would require a more detailed and accurate geologic map of the city.

The authors returned to Haiti in late April 2010 to perform additional in-depth field studies of geotechnical-driven damage patterns and soil liquefaction from the earthquake. This research was funded by an NSF Rapid Response Research (RAPID) proposal and included detailed geologic mapping of Port-au-Prince and shear wave velocity profiling throughout the city as two primary goals. Later, the United Nations Development

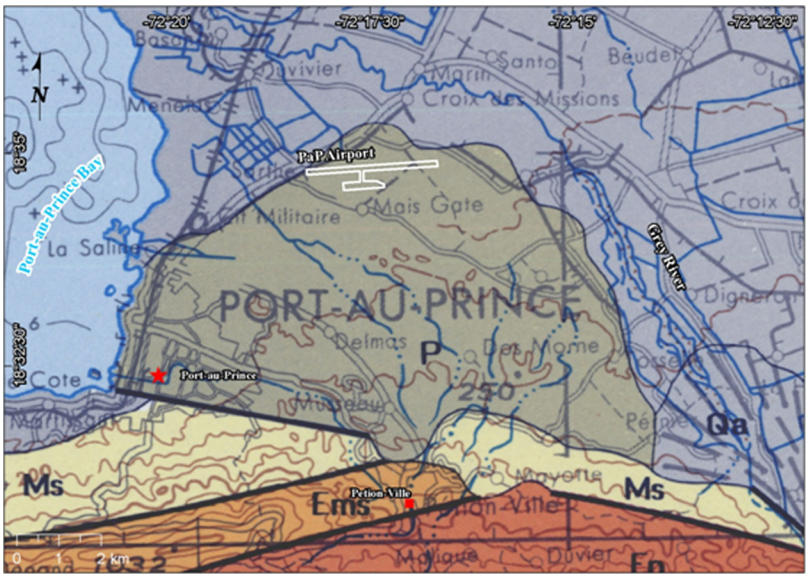

Figure 1. Previously published regional geologic map including Port-au-Prince, Haiti (modified from Lambert et al. 1987).

Programme (UNDP) became interested in this effort and provided some additional funding for map development and dissemination to government and nongovernmental organizations in Haiti. The new Port-au-Prince geologic map culminating from this work is presented in Figure 2. The new map is based on field reconnaissance mapping and geomorphic interpretation of a 10-m (spatial resolution) DEM. The DEM was obtained from an airborne light detection and ranging (LiDAR) survey funded by the World Bank, coordinated by ImageCat, and performed by the Rochester Institute of Technology (http://ipler.cis.rit.edu/projects/haiti). A free geographic information system (GIS) version of the new Port-au-Prince geologic map is available from UNDP (please contact the lead author via e-mail for details on how to obtain it). Descriptions of the new geologic map units and details about how the geologic boundaries were established are provided below.

The Port-au-Prince region is a physiographically diverse area that has undergone a complex geologic history of tectonism, erosion, and sedimentation within an area of regional deformation associated with the active Enriquillo-Plantain Garden fault zone (EPGFZ) and other associated secondary faults. The EPGFZ is located approximately 5 to 7 km south of Port-au-Prince. This section of the fault did not rupture during the 12 January 2010 earthquake (the epicenter was approximately 30 km to the west), but has geomorphic expression consistent with Holocene-active faulting. Other potentially active faults and folds associated with the EPGFZ trend west-northwesterly at the mountain range front and low hills in the southern part of the study area. These secondary faults may be "flower structures" that connect at depth with the main EPGFZ, and accommodate some of the local tectonic deformation by strain partitioning. Several of these faults cut through the Pliocene fan deposits with a northwestward trend that are subparallel with local folds and warps in the fans (refer to

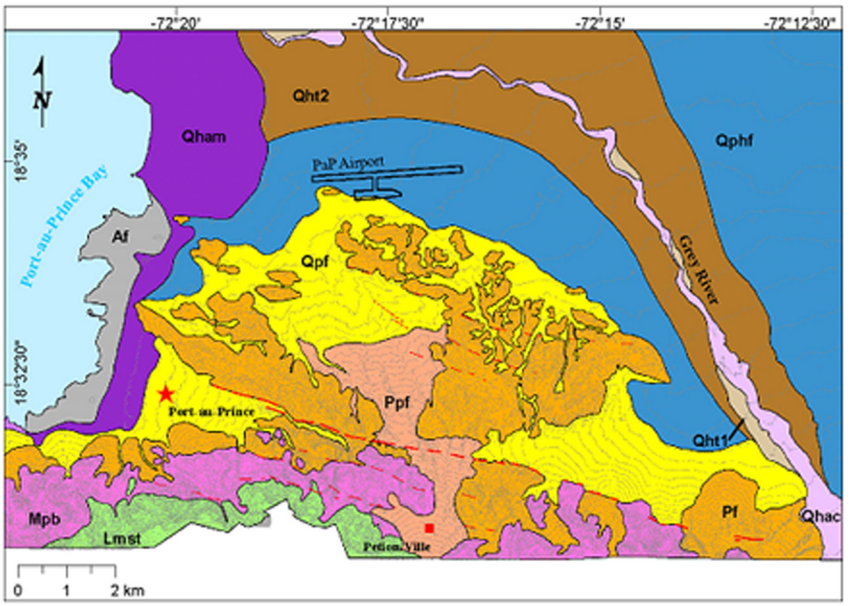

Explanation

Af	Artificial fill forming reclaimed land west of the mapped 1785 shoreline
Qhac	Stream channel alluvium; typically well-sorted, bedded, unconsolidated sand, silty sand, and gravel within the active channels of major streams
Qham	Marine/estuarine deposits interfingered with alluvial fan deposits and local fill
Qht1	Lower alluvial terrace deposits/surfaces within areas of historic flood inundation
Qht2	Elevated alluvial terrace deposits/surfaces bordering major streams and margins of intermontane valleys
Qphf	Alluvial fan/plain deposits
Qpf	Fan deposits forming steep fans at the rangefront
Ppf	Broad, deeply incised strath surface (or thin deposit veneer) developed over Pliocene fan
Pf	Pliocene fan deposits forming a deeply dissected paleofan complex along the rangefront
Mpb	Fanglomerate/talus deposits consisting of coarse, angular "breccia"
Lmst	Limestone bedrock exposed along rangefront

Faults - Long dashes indicate relatively high degree of confidence on location
Short dashes express less certain location

Inferred primary fault cutting Mio-Pliocene fan deposits

Inferred secondary fault cutting Mio-Pliocene fan deposits

Figure 2. New geologic map of Port-au-Prince, Haiti. Note: a free geographic information system (GIS) version of this map is available from the United Nations Disaster Programme (UNDP). (Contact the lead author via e-mail for details on how to obtain it.)

Figure 2). These faults appear to be reverse oblique/strike slip faults that have steep dips (as evidenced by relatively straight map patterns) that uplifted the fan deposits in the late Pliocene and Pleistocene. Shortening in this zone indicates a significant component of transpression along this segment of the main trace of the fault as predicted by GPS studies.

The faults in Figure 2 were mapped by a combination of geomorphic interpretation (linear valleys, aligned saddles in ridges), truncations/contacts between geologic units, and extrapolations of faults observed in roadcuts. An apparent left lateral displacement of a late Pliocene/Pleistocene paleodrainage surface (map unit Ppf) near Pétion-Ville, and possible subtle scarps and offsets in Pleistocene and Holocene alluvium, suggest that these faults may be Holocene active. If verified to be potentially active, these faults could represent possible local earthquake sources or zones of surface fault deformation that warrant further consideration and hazard evaluation.

The general topography within the study area includes a steep mountain range front south of the greater Port-au-Prince urban area formed in Miocene and older bedrock, and moderate-to-steep bedrock ridges and hills in Mio-Pliocene clastic and carbonate sedimentary rock north of the mountain range. The ridges and hills extend into the eastern and central part of Port-au-Prince (e.g., Delmas), and are deeply incised by streams with narrow intermountain valleys. Gently sloping alluvial plains and fans surround the hills and underlie the urbanized core of the city and the airport area. The central district of Port-au-Prince occupies a relatively flat coastal plain underlain by alluvial and marine-estuarine sediments, and reclaimed land that extends westward to the port area and modern shoreline.

Miocene limestone bedrock (Lmst) forms the steep mountain front along the south margin of our study area. Areas of limestone were identified in the field by outcrops and roadcut exposures, and geomorphically by relatively uniform, steep slopes. The white limestone is massively to thickly bedded, and quite dense and hard. Little of the greater Port-au-Prince population center is built on the Lmst deposits.

North of the Lmst unit, at the base of the range front, is a band of Mio-Pliocene "fanglomerate/breccias" ("breccias," Mpb) comprised of dense (often rings with hammer blows) angular limestone blocks, variably cemented in a finer-grained sandy and calcareous matrix. The fragments are variably clast- or matrix-supported. Crude beds and layering in the breccias are generally thick to massive. This unit appears to represent an old Miocene-Pliocene talus/fan that buttressed the range front and has become cemented by carbonate over time. These deposits are deeply dissected and typically strong enough to form moderately steep to steep slopes and narrow, rounded-spur ridges projecting northward into the valley. The Mpb is reddened and weathered/oxidized, with variable thickness and, in many locations, covered with residual soil and colluvium. Extensive development has occurred on the Mpb unit breccias, including *bidonvilles* that cover many ridge crests and slopes.

A large Pliocene fan (Pf) complex extends northward from the Mio-Pliocene breccia at the range front and forms low hills and ridges through the eastern part of Port-au-Prince and adjacent suburbs. The Pf unit is comprised of crudely bedded siltstone, sandstone, claystone, conglomerate, and localized limestone with some zones of dense unlithified sand or very stiff clay. These deposits are locally referred to as the "Delmas formation." Thick, oxidized residual soils are developed on these deposits. The Pliocene fan sediments were

originally deposited on a large fan that prograded outward from the range front into the valley, and the sediment grain size generally becomes finer towards the distal ends of the ancient fan. The sediments deposited in the fan were derived from the reworking of eroded Mio-Pliocene breccias and fluvial sediments from ancestral streams draining the mountains to the south. Pliocene fan deposits are defined geomorphically by moderately steep slopes, broad ridges, and incised drainage networks within a fan-shaped series of hills in the southern and central part of the study area (including the Pétion-Ville and Delmas areas).

Surficial Pf deposits are typically dense and weakly to moderately cemented, with a character typical of "soft rock" conditions. The individual beds in the Pliocene fan are generally several meters to tens-of-meters thick with an estimated composite thickness of many tens to hundreds of meters. Regional uplift associated with the EPGFZ and the local faults have tilted and raised the Pliocene fan deposits, and beds in some areas of the fan are tilted (dip) between 20 and 35 degrees. Subsequent erosion of the Pliocene fan has resulted in the deeply dissected morphology around Port-au-Prince and the ridge-and-swale topography that has been densely developed along the southern and eastern margins of the city.

A large, flat surface was eroded into the central part of the Pliocene fan surface (Pétion-Ville area) by an ancestral stream, and this is a beveled strath (erosional) surface rather than a depositional fan deposit. The planated surface is designated Ppf on the geologic map, indicating that it is an assumed Pleistocene surface. The deposits underlying this unit are essentially the same as those underlying the Pliocene fan. An important aspect of the planated fan is that it is an area of local lower relief within the Pliocene fan. This surface also exhibits a possible long-term left lateral displacement along one of the mapped secondary faults associated with the EPGFZ, suggesting that significant past left-lateral displacement has occurred along this fault.

A sequence of Pleistocene fans (Qpf) and Pleistocene-Holocene stream terraces (Qphf) surround the Pliocene fan, extend along the margins of stream and river valleys, and propagate outward into the valley and toward the shoreline. These geologic units consist of sediment derived by erosion of the older Pf and Mpb units, with contribution of sediment from streams draining from the range front. These Pleistocene fans and terrace deposits have also been uplifted since deposition, resulting in the deep incision of tributary streams. These streams are routed in concrete-lined channels through the urban center of Port-au-Prince, but where unlined, the sidewalls of stream channels are typically nearly vertical and expose dense interbedded sand, silty sand, gravel, and cobbles that are reddened in places and exhibit some weak cementation. Much of the development on low gradient sloping areas surrounding the central district of Port-au-Prince has occurred over these Pleistocene deposits. Pleistocene fan deposits form distinctive geomorphic landforms that show up clearly in the DEM. Pleistocene-Holocene stream terraces are defined in the DEM as elevated valleys and broad benches bordering the Grey River and its major tributaries.

The central district of Port-au-Prince occupies a narrow, Holocene coastal alluvial plain (Qham) bounded to the east by the Qpf fans or Pf hills, and extending to the shoreline. Alluvial deposits underlying this coastal plain were deposited in a marine margin setting, and include interbedded terrestrial alluvium and estuarine muds with a high organic content. These materials represent the youngest natural geologic materials in the study area. The groundwater table in this unit is shallow, typically within one to several meters of the

ground surface. The coastal plain is expressed on the DEM as a broad, low relief plain adjacent to the coastline, and much of the central district of Port-au-Prince is located on this unit.

Artificially filled (Af) ground extends west of the original shoreline location in the central district of the city. We defined the contact between the natural Holocene Qham deposits and filled ground based on the mapped 1785 shoreline as shown on a historic map from Ponce (1791). The fill was placed progressively in separate stages of filling and development over the course of several hundred years. As a result, the fill is heterogeneous in texture and density, and includes some low-density zones. Liquefaction and lateral spreading were documented in some Af deposits during the earthquake, particularly those closest to the current coastline (Green et al. 2011, Olson et al. 2011).

Holocene fluvial alluvium (Qhac) has been differentiated principally along the Grey River and its major tributaries in the study area. It typically occurs under river channels and active alluvial floodplains and low areas. Modern stream banks expose these deposits that typically consist of interbedded sand, silty sand, and silt with some gravel lenses in the upper reaches of stream valleys, and sandy silt, silt, and silty clay along the coastal discharge areas of streams. Some liquefaction occurred in this unit (Olson et al. 2011), but was primarily confined to the most recent stream deposits/terraces (Qht1) along the distal reach of the Grey River near the coast, where the Holocene stream deposits are dominated by sand, silt, and fine gravel. The early Holocene to Pleistocene terrace (Qht2) and fan deposits (Qphf) are quite dense/stiff, elevated above the ground water table, or gently sloping without free faces, and therefore resistant to liquefaction and lateral spreading.

SHEAR WAVE VELOCITY PROFILES IN PORT-AU-PRINCE

The authors conducted MASW testing at 36 sites in and around Port-au-Prince, Haiti from 19–25 April 2010 as a means to rapidly and non-intrusively obtain V_S profiles across the city. Table 2 and Figure 3 provide the coordinates and map locations of the MASW surveys, respectively. Potential test locations initially were laid out on a 1.5-km grid pattern to provide adequate coverage of the city. These locations were then adjusted to target aftershock ground motion stations and areas of interest where strong site effects (either soft-soil or topographic amplification) were suspected based on the prior GEER reconnaissance and analysis of damage statistics (Rathje et al. 2011). Attempts were also made to perform tests on various geologic units to facilitate microzonation. However, the refined geologic map was not available at the time of field testing, so coverage of some geologic units was limited. Congestion and rubble made finding optimal test locations within the city difficult, resulting in further manipulation of the planned test locations. When aftershock station sites were tested, the surveys were completed within 100 m of the instruments whenever possible.

The MASW method (Park et al. 1999, Zywicki 1999, Foti 2000) has been used extensively over the past decade to determine near-surface V_S profiles for engineering applications (e.g., Xia et al. 2002, Socco and Strobbia 2004, Foti 2005, Rix 2005, Tran and Hiltunen 2008, Cox and Wood 2010, Park and Carnevale 2010). All of the MASW surveys performed for this study were completed using a linear array of 24 receivers (4.5-Hz geophones) with a constant receiver spacing of approximately 1 m (total array length of 23 m).

Table 2. Seismic site classifications for surface wave test locations (TL) in Port-au-Prince, Haiti

TL#	Latitude	Longitude	V_{S30} (m/s)	NEHRP Site Class	Geology
1*	18.53288	−72.38046	216	D	***
2	18.52979	−72.39187	495	C	***
3	18.53542	−72.40527	641	C	***
4	18.54284	−72.40181	656	C	***
5	18.53406	−72.36319	246	D	Af
6	18.54650	−72.41879	614	C	***
7	18.52704	−72.33746	436	C	Mpb
8	18.54389	−72.33897	506	C	Qpf
9	18.56683	−72.32314	518	C	Qpf
10	18.53551	−72.32486	523	C	Qpf
11	18.54858	−72.33829	426	C	Qpf
12	18.52984	−72.33065	949	B	Pf
13	18.54989	−72.32732	385	C	Qpf
14*	18.56276	−72.33847	303	D	Qham
15*	18.55379	−72.30407	451	C	Qpf
16*	18.56238	−72.29709	427	C	Pf
17	18.57405	−72.29540	452	C	Qpf
18	18.54948	−72.28960	504	C	Ppf
19*	18.52910	−72.30849	505	C	Pf
20*	18.52221	−72.29942	476	C	Mpb
21*	18.52693	−72.29783	626	C	Mpb
22	18.51910	−72.27383	767	B/C	Pf
23*	18.50353	−72.30606	1014	B	Lmst
24	18.53904	−72.31709	577	C	Pf
25	18.54717	−72.25330	566	C	Pf
26	18.54064	−72.22699	**	**	Qht1
27	18.60721	−72.27852	346	D	Qht2
28	18.53812	−72.28190	511	C	Pf
29*	18.56596	−72.24897	484	C	Qphf
30	18.57244	−72.26693	469	C	Qphf
31*	18.53927	−72.30951	473	C	Pf
32	18.54162	−72.33354	619	C	Qpf
33	18.55056	−72.34634	232	D	Af
34	18.55727	−72.35144	356	C/D	Af
35	18.54734	−72.34016	348	D	Qham
36	18.53999	−72.34530	343	D	Qham

*Location of aftershock ground motion station
**MASW data could not be interpreted
***Geology unknown at these test locations

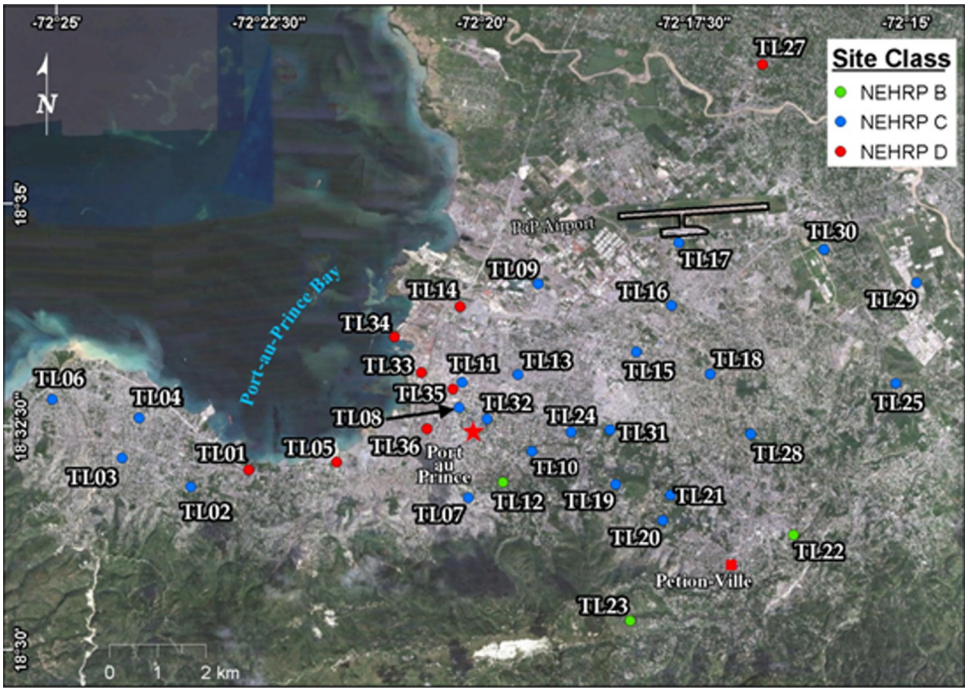

Figure 3. Locations and names of sites in Port-au-Prince, Haiti where multichannel analysis of surface waves (MASW) testing was performed to obtain shear wave velocity profiles (image courtesy of Google Earth, ©2009 Google).

Three separate source-offset distances (i.e., the distance from the source to the first receiver in the array) of approximately 5-, 10-, and 20-times the receiver spacing were used at each site.

A 7.3-kg sledgehammer was used as the dynamic source and signals from at least five impacts were averaged at each source location. The hammer was struck directly on the ground surface when testing on stiff surficial material, while a steel plate was struck when testing on soft materials.

Surface wave dispersion curves were generated from the raw experimental data using a frequency domain beamformer method (Zywicki 1999, Zywicki and Rix 2005). The individual dispersion curves from each source-offset distance were compared as a means to identify possible near-field effects in the dispersion data and to aid in selecting the fundamental mode of surface wave propagation. The three individual sets of dispersion data also provided a more robust means for estimating dispersion uncertainty (Cox and Wood 2011). For this work, the experimental data at each site was divided into 30 wavelength bins. The mean phase velocity and associated uncertainty on the mean were then calculated for each bin (Figure 4a). A fundamental mode inversion was used to fit a theoretical dispersion curve to the experimental data in order to obtain the V_S profile for the site (Figure 4b). The shear

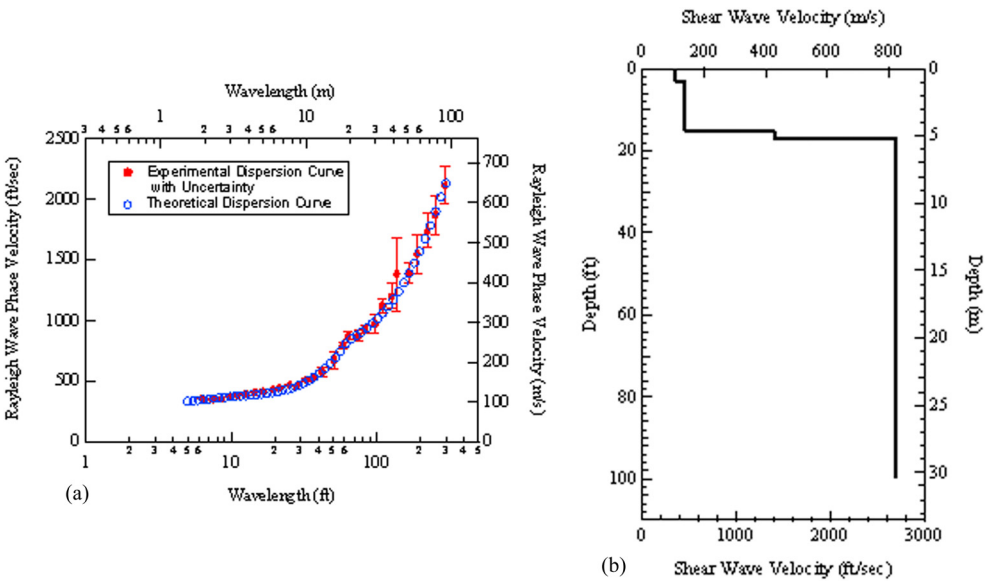

Figure 4. Multichannel analysis of surface waves (MASW) results for test location 17 (TL#17): (a) experimental dispersion curve with uncertainty and associated theoretical dispersion curve, and (b) shear wave velocity profile corresponding to theoretical dispersion curve.

wave velocity profiles obtained from the inversions for each site were all limited to a depth of approximately 30 m, which was always less than the maximum experimental wavelength divided by two (i.e., $\lambda_{max}/2$).

The V_S profiles for each test location (TL) are provided in Table 3 so that interested readers can use them for more detailed studies (e.g., site amplification, etc.) if desired. The V_S profile for TL#26 is not included because the data at this site was of poor quality and the fundamental mode of propagation could not be determined. The V_{S30} values for each site are provided in Table 2. These values were used to determine the NEHRP (BSSC 2003) site classifications for each test location. The test locations have been color-coded according to NEHRP Site Class in Figure 3 with green representing Site Class B, blue representing Site Class C, and red representing Site Class D. The relationships between V_{S30} values and surficial geologic unit are discussed below.

RELATIONSHIPS BETWEEN V_{S30} VALUES AND SURFICIAL GEOLOGY

The V_S profile locations are shown relative to the newly developed geologic map of Port-au-Prince in Figure 5. The surficial geologic units for most of the test locations are also indicated in Table 2. The surficial geology for the five sites near Carrefour (TL#1–4 and TL#6, refer to Figure 3) has not yet been determined. As such, these sites are not included in the subsequent velocity-geology relationships.

Table 3. Shear wave velocity profiles for surface wave test locations (TL) in Port-au-Prince, Haiti

TL#1		TL#2		TL#3		TL#4		TL#5		TL#6		TL#7	
Depth (m)	V_S (m/s)	Depth (m)	V_S (m/s)	Depth (m)	V_S (m/s)	Depth (m)	V_S (m/s)	Depth (m)	V_S (m/s)	Depth (m)	V_S (m/s)	Depth (m)	V_S (m/s)
0.0	100	0.0	240	0.0	340	0.0	300	0.0	0300	0.0	2400	0.0	300
0.9	100	1.8	240	2.4	340	2.1	300	0.9	20	2.1	200	1.5	300
0.9	70	1.8	400	2.4	530	2.1	4530	0.9	260	2.1	340	1.5	320
2.9	70	6.4	400	4.3	530	5.2	430	2.4	260	4.7	340	6.7	320
2.9	160	6.4	350	4.3	370	5.2	550	2.4	120	4.7	610	6.7	440
9.0	160	12.5	350	5.2	370	12.2	5350	9.8	120	16.9	610	10.4	440
9.0	320	12.5	720	5.2	430	12.2	940	9.8	370	16.9	1220	10.4	460
30.5	320	30.5	720	10.7	430	30.5	940	30.5	370	30.5	1220	25.6	460
				10.7	910							25.6	640
				30.5	910							30.5	640

TL#8		TL#9		TL#10		TL#11		TL#12		TL#13		TL#14	
Depth (m)	V_S (m/s)	Depth (m)	V_S (m/s)	Depth (m)	V_S (m/s)	Depth (m)	V_S (m/s)	Depth (m)	V_S (m/s)	Depth (m)	V_S (m/s)	Depth (m)	V_S (m/s)
0.0	110	0.0	240	0.0	240	0.0	230	0.0	400	0.0	150	0.0	180
1.3	110	1.2	240	1.5	240	240	230	3.0	400	0.9	150	0.9	180
1.3	270	1. 2	300	1.5	370	230	280	3.0	9270	0.9	120	0.9	270
3.3	270	3.0	300	4.3	370	9.0	280	9.1	1070	2.1	120	2.4	270
3.3	660	3.0	200	4.3	380	9.0	460	9.1	760	2.1	220	2.4	160
30.5	660	4.6	200	7.6	380	12.0	460	15.5	760	6.9	220	9.1	160
		4.6	440	7.6	6440	12.0	600	15.5	1370	6.9	430	9.1	460
		11.7	440	30.5	640	30.5	640	30.5	1370	430	430	30.5	460
		11.7	790							13.0	530		
		30.5	790							20.7	530		
										20.7	790		
										30.5	790		

TL#15		TL#16		TL#17		TL#18		TL#19		TL#20		TL#21	
Depth (m)	V_S (m/s)	Depth (m)	V_S (m/s)	Depth (m)	V_S (m/s)	Depth (m)	V_S (m/s)	Depth (m)	V_S (m/s)	Depth (m)	V_S (m/s)	Depth (m)	V_S (m/s)
0.0	180	0.0	150	0.0	110	0.0	180	0.0	230	0.0	230	0.0	190
1.5	180	1.2	180	0.9	110	0.9	180	1.5	230	1.8	230	1.5	190
1.5	220	1.2	420	0.9	140	0.9	340	1.5	350	1.8	380	1.5	310
4.6	220	12.2	220	4.6	140	2.7	340	7.6	350	4.3	380	4.0	310
4.6	340	12.2	200	4.6	430	2.7	340	7.6	580	4.3	180	4.0	580
10.7	340	14.3	200	5.2	430	12.5	440	25.9	580	5.3	180	16.2	580
10.7	640	14.3	610	5.2	820	12.5	640	25.9	980	5.3	450	16.2	1220

Table 3. *Continued*

TL#15		TL#16		TL#17		TL#18		TL#19		TL#20		TL#21	
Depth (m)	V_S (m/s)	Depth (m)	V_S (m/s)	Depth (m)	V_S (m/s)	Depth (m)	V_S (m/s)	Depth (m)	V_S (m/s)	Depth (m)	V_S (m/s)	Depth (m)	V_S (m/s)
25.9	640	30.5	610	30.5	820	30.5	640	30.5	980	17.5	450	30.5	1220
25.9	1370									17.5	780		
30.5	1370									30.5	780		

TL#22		TL#23		TL#24		TL#25		TL#26		TL#27		TL#28	
Depth (m)	V_S (m/s)	Depth (m)	V_S (m/s)	Depth (m)	V_S (m/s)	Depth (m)	V_S (m/s)	Depth (m)	V_S (m/s)	Depth (m)	V_S (m/s)	Depth (m)	V_S (m/s)
0.0	610	0.0	300	0.0	300	0.0	360	0.0	170	0.0	400	0.0	140
7.6	610	1.5	300	2.1	300	1.5	360	4.3	170	2.7	400	1.1	140
7.6	700	1.5	760	2.1	780	1.5	410	4.3	220	2.7	590	1.1	190
21.3	700	9.4	760	4.9	780	7.9	410	8.8	220	7.0	590	2.3	190
21.3	1190	9.4	1370	4.9	160	7.9	650	8.8	260	7.0	150	2.3	370
30.5	1190	27.7	1370	5.9	160	14.0	650	14.9	260	9.6	150	4.1	370
		27.7	2290	5.9	660	14.0	460	14.9	820	9.6	730	4.1	460
		30.5	2290	21.2	660	20.1	460	30.5	820	30.5	730	10.2	460
				21.2	760	20.1	930					10.2	660
				30.5	760	30.5	930					30.5	660

TL#30		TL#31		TL#32		TL#33		TL#34		TL#35		TL#36	
Depth (m)	V_S (m/s)	Depth (m)	V_S (m/s)	Depth (m)	V_S (m/s)	Depth (m)	V_S (m/s)	Depth (m)	V_S (m/s)	Depth (m)	V_S (m/s)	Depth (m)	V_S (m/s)
0.0	270	0.0	180	0.0	290	0.0	370	0.0	320	0.0	180	0.0	180
1.2	270	0.9	180	2.1	290	0.9	370	2.0	320	1.5	180	2.1	180
1.2	190	0.9	300	2.1	530	0.9	90	2.0	190	1.5	220	2.1	160
2.4	190	6.1	300	7.3	530	5.8	90	5.9	190	4.9	220	2.7	160
2.4	370	6.1	630	7.3	590	5.8	240	5.9	370	4.9	310	2.7	290
10.4	370	16.8	630	14.0	590	16.5	240	21.2	370	18.6	310	14.9	290
10.4	490	16.8	470	14.0	790	16.5	430	21.2	550	18.6	590	14.9	490
20.4	490	27.4	470	30.5	790	30.5	430	30.5	550	30.5	590	30.5	490
20.4	850	27.4	1130										
30.5	850	30.5	1130										

Note: MASW data at TL#26 could not be interpreted

With the exception of the Qhac and Qht1 units, which occupy narrow strips of land adjacent to the Grey River that runs along the eastern and northern sides of Port-au-Prince, all significant units on the new geologic map contain at least one V_S profile. The number of V_S profiles range from one, for the Ppf, Qht2, and Lmst units, to eight, for the Pf and Qpf units. While not ideal coverage in terms of surficial geology, we note that the new geologic map was not developed until after the field V_S profiling was completed. Furthermore, time and

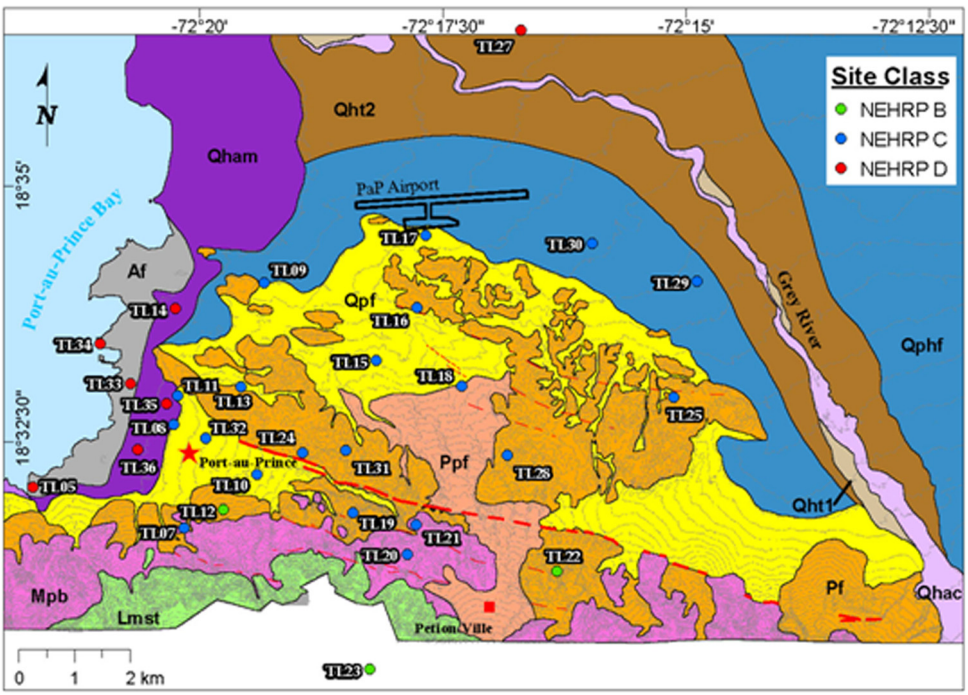

Figure 5. Locations and names of sites in Port-au-Prince, Haiti where surface wave testing was performed to obtain shear wave velocity profiles. Shown relative to the new geologic map of Port-au-Prince developed in this study.

logistical constraints limited the number of sites that could reasonably be tested. Despite these shortcomings, the information presented herein provides a good base for an initial seismic site classification microzonation of Port-au-Prince that can be expanded and refined as additional information is collected.

Borehole and deep geophysical data were not readily available to evaluate the thicknesses of the various geologic units. Based on limited exposures and geologic map interpretation, the Pleistocene and Holocene geologic deposits are probably on the order of tens-of-meters thick, and Mio-Pliocene deposits are probably on the order of many tens-of-meters to several hundred meters thick. However, local variability could be significant, complicating depth correlations between the velocity profiles and geologic units. Subsurface investigations and refined depth correlations between shear wave velocity and geologic unit would be useful to develop higher resolution microzonation maps during future studies.

The individual V_S profiles, median V_S profile with $+/-$ one standard deviation, and coefficients of variation (COV) as a function of depth for geologic units Af, Qham, Qphf, Qpf, Pf, and Mpb are presented in Figures 6–11, respectively. In general, COV values for the geologic units are greatest near the surface and decrease with depth. This is believed to be a result of variable surficial weathering (intensity and thickness) across the units. A few exceptions to this generality are noted when the depth and stiffness of underlying rock vary

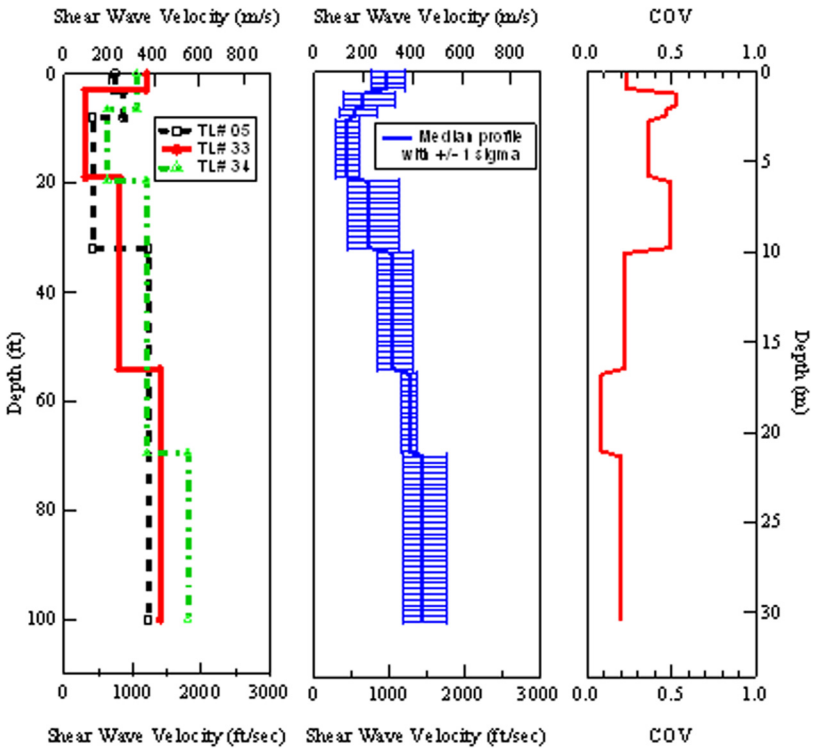

Figure 6. Surficial geologic unit Af: (a) individual V_S profiles, (b) median V_S profile with $+/-$ one standard deviation, and (c) coefficient of variation.

significantly between profiles within the same surficial geologic unit, such as in Figure 11 for the Mpb unit. The V_{S30} values calculated from the median V_S profile in each geologic unit are presented in Table 4. The number of V_S profiles used to develop the median V_S profile for each geologic unit and the NEHRP site classifications are also provided. We note that the V_S profile for TL#12 was not used to determine the median V_S profile for the Pf unit, as it was judged to be unrepresentative of the entire unit due to its anomalously high velocities (refer to Tables 2 and 3). The MASW dispersion data at this site was initially suspected to be dominated by higher-mode surface wave propagation, giving the impression of a much stiffer subsurface. However, the validity of the dispersion data was confirmed by an independent test method (the spectral analysis of surface waves method, or SASW method) on a subsequent trip to Haiti. Therefore, it is believe that TL#12 is an isolated area of stiffer/unweathered limestone. It is possible that other isolated areas like this exist in the mapped Pf unit.

It is interesting to compare the median V_S profiles for each geologic unit with the same seismic site classification. The NEHRP Site Class D median profiles for geologic units Af, Qham, and Qht2 are compared in Figure 12a. The total number of individual V_S profiles in each unit is indicated in parentheses in the legend. The median V_S profiles for the Af and

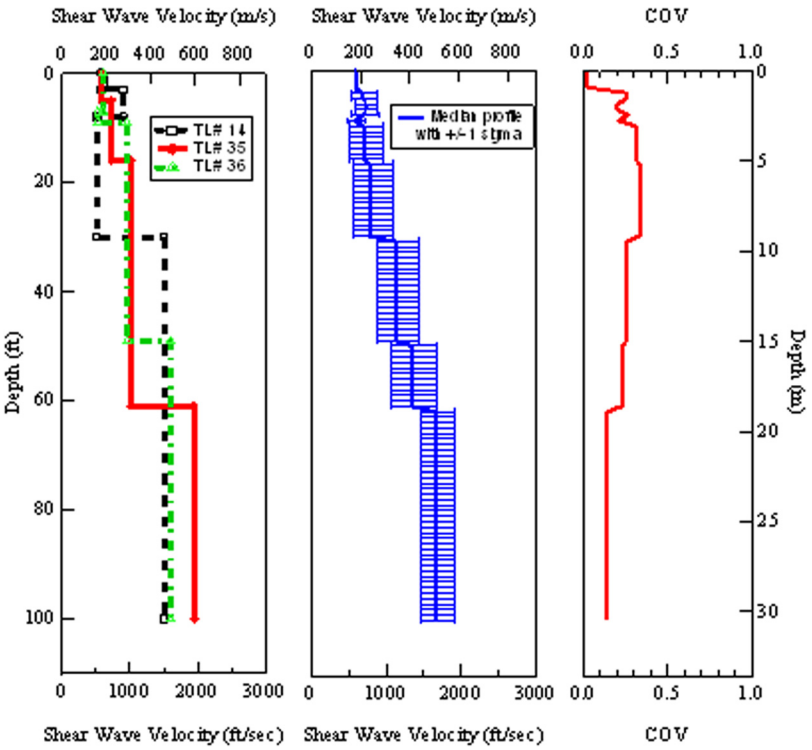

Figure 7. Surficial geologic unit Qham: (a) individual V_S profiles, (b) median V_S profile with $+/-$ one standard deviation, and (c) coefficient of variation.

Qham units are remarkably similar. The V_S profile for the Qht2 unit is also very similar until an abrupt impedance contrast (rock) is encountered at a depth of 15 m. While the profiles from all three of these units yield Site Class D classifications, it is obvious that the strong impedance contrast in the Qht2 unit would result in a very different site response. For example, a simple transfer function for uniform, damped soil over elastic bedrock (Kramer 1996) can be used to estimate the linear response of varying thicknesses of this soil ($V_S \sim 300$ m/s, assumed 5% damping) over rock ($V_S \sim 800$ m/s, assumed 0.5% damping). The peak amplitude of the transfer function is controlled by the shear wave velocity, damping ratio, and density contrasts between soil and underlying rock, and is not influenced by the thickness of the soil. Therefore, it is a constant (approximately 2.4) for the conditions described. However, as the thickness of the soil layer increases from 15 m to 30 m to 50 m, the first mode natural frequency of the soil profile decreases from 4.8 Hz to 2.4 Hz to 1.5 Hz, respectively.

Since bedrock was not encountered in the top 30 m in the Qham and Af units, it is likely that these units amplified frequencies less than 2.5 Hz (periods longer than 0.4 sec), while the Qht2 unit likely amplified frequencies around 5 Hz (periods around 0.2 sec). Additional V_S profiling is needed in the Qht2 unit to determine if this shallow impedance contrast is

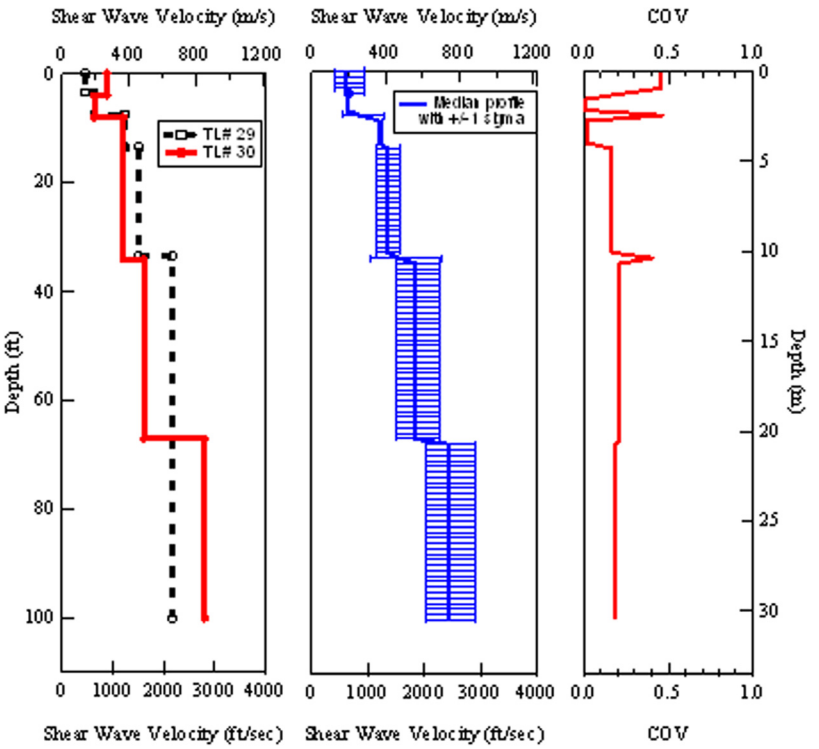

Figure 8. Surficial geologic unit Qphf: (a) individual V_S profiles, (b) median V_S profile with $+/-$ one standard deviation, and (c) coefficient of variation.

present throughout. This simple example illustrates the well-known limitations of a site classification system based solely on V_{S30}.

We also note that one of the three V_S profiles used in developing the Af median V_S profile (TL#34, collected at the seaport) has a V_{S30} value about 100 m/s greater than the other two Af profiles (TL#5 and TL#33, both collected approximately 0.3 km from the coastline). Considering the individual V_S profiles (Figure 6), TL#5 and TL#33 have soft soils (V_S less than about 125 m/s) that are relatively thick (greater than about 5 m), while TL#34 has somewhat stiffer soils ($V_S = 190$ m/s) that are less than 4 m thick and are overlain by a stiffer near-surface layer composed of engineered fill at the port. The shear wave velocity profile at the port is likely not representative of profiles further inland within the Af unit because of the presence of hydraulic fill overlain by compacted fill. Therefore, the median V_{S30} value for Af in Table 4, which was computed from all three profiles, may be slightly high, but it is still well within the V_{S30} bounds of NEHRP Site Class D. Finally, depending on the characteristics of the low velocity layers encountered at TL#5 and TL#33 (i.e., soft clay or liquefiable soils), it is possible that these sites would classify as Site Class E or F.

The NEHRP Site Class C median V_S profiles for geologic units Qpht, Ppf, Pf, Mpb, and Qpf are similarly compared in Figure 12b. Again, the total number of individual V_S profiles

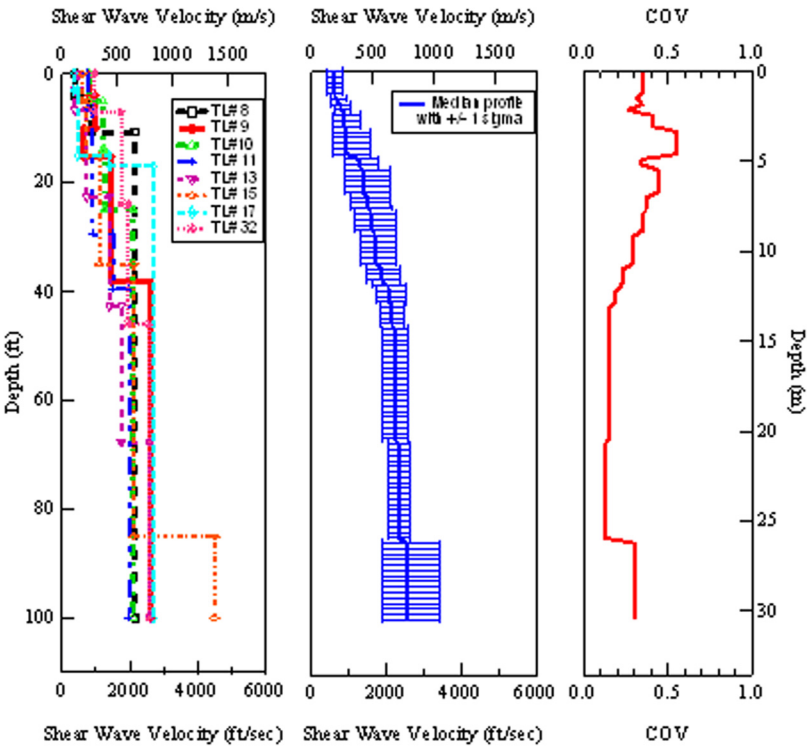

Figure 9. Surficial geologic unit Qpf: (a) individual V_S profiles, (b) median V_S profile with $+/-$ one standard deviation, and (c) coefficient of variation.

in each unit is indicated in parentheses in the legend. The median V_S profiles for all of these units are very similar and, on average, no major differences in site response would be expected based on the profile shapes. However, the smoothing that takes place during calculation of the median profile tends to mask sharp impedance contrasts that could control local site effects. The median V_{S30} values within these units (Table 4) only range from 480 to 564 m/s, placing them well within the bounds of NEHRP Site Class C. As a result, it is likely that most sites located within these geologic units classify as NEHRP Site Class C. The only outliers are TL#12 (previously discussed) and TL#22 in the Pf unit. TL#12 is a firm Site Class B ($V_{S30} = 949$ m/s), while TL#22 is a borderline Site Class B/C ($V_{S30} = 767$ m/s).

The median V_S profiles for all geologic units are compared in Figure 13. It is obvious that the Lmst unit (NEHRP Site Class B) is significantly stiffer than the other units. However, only one V_S profile was obtained in Lmst and further testing should be performed in this unit to confirm this observation. At this scale, it is still possible to distinguish between the NEHRP C and D profiles, but the differences are not as obvious. Of particular interest is the Qht2 profile discussed above in regards to Figure 12a. Despite classifying as NEHRP Site Class D, this profile appears to be a hybrid between the NEHRP Site Class D and Site

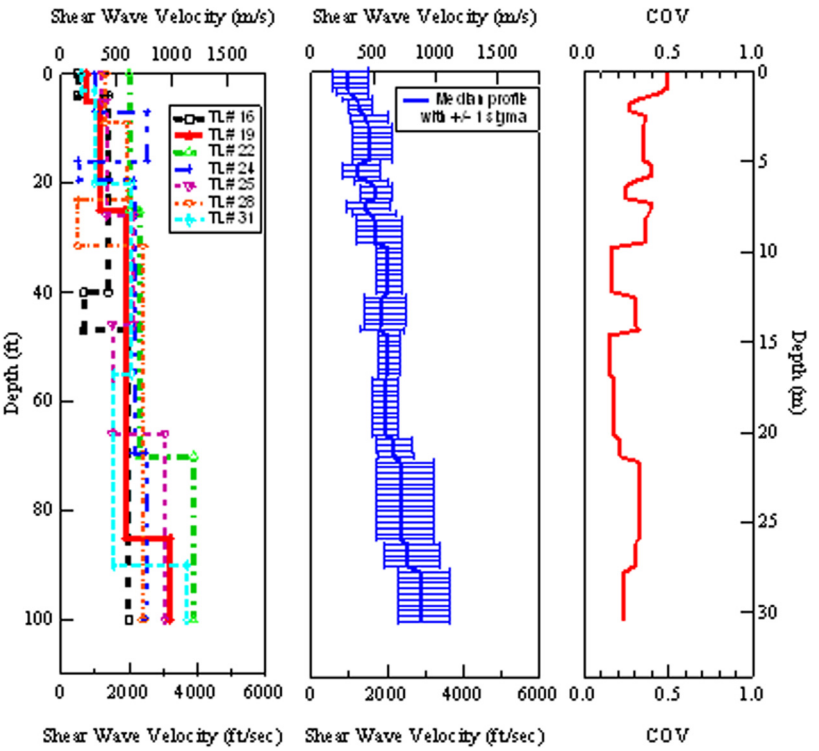

Figure 10. Surficial geologic unit Pf: (a) individual V_S profiles, (b) median V_S profile with $+/-$ one standard deviation, and (c) coefficient of variation.

Class C profiles. The surficial material is quite soft and similar to units Af and Qham to a depth of approximately 15 m, below which V_S increases abruptly to align with the stiffer Site Class C profiles. As noted above, this unit needs additional V_S profiling to determine if this is a representative trend.

SEISMIC SITE CLASSIFICATION MAP FOR PORT-AU-PRINCE

The median V_S profiles and corresponding V_{S30} values presented above for each geologic unit allow a preliminary seismic site classification microzonation map to be developed for the Port-au-Prince area. The site classification map developed from this work is presented in Figure 14. Only a small portion of the mapped area classifies as NEHRP Site Class B. Much of the greater Port-au-Prince area classifies as Site Class C or D, based strictly on V_{S30}. However, it should be stressed that some areas within the mapped Holocene alluvial deposits and coastal artificial fills may classify as Site Class E or F, depending on local subsurface conditions (e.g., presence of soft clay or liquefiable soil) that cannot be determined solely with V_S profiling. Therefore, the map conservatively assigns a Site Class D/E classification to all geologic units that classified as Site Class D based strictly on V_{S30}. The legend for the map reminds the user that: "Soils within this zone may classify as either Site Class D

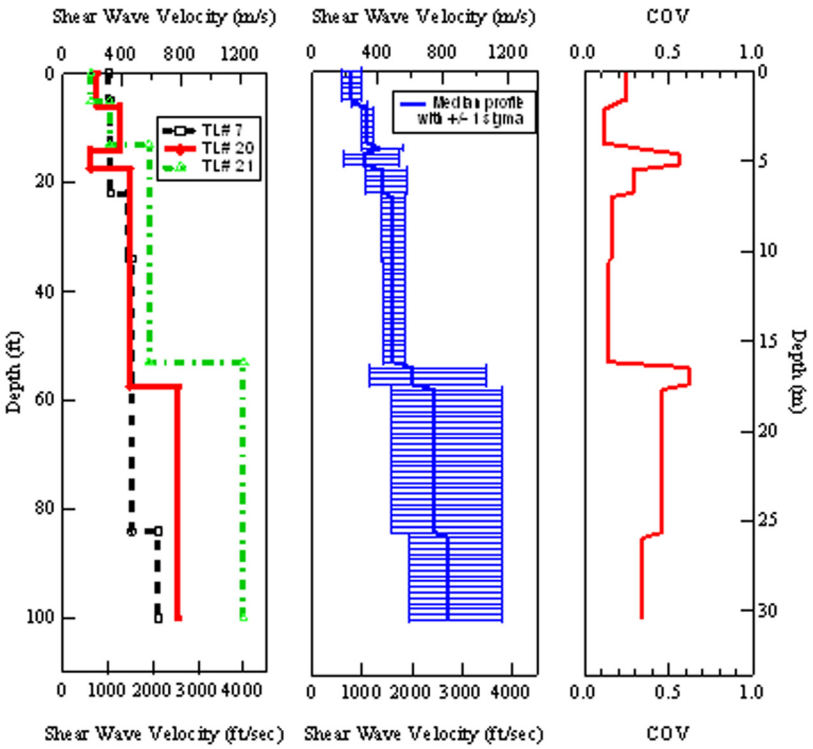

Figure 11. Surficial geologic unit Mpb: (a) individual V_S profiles, (b) median V_S profile with $+/-$ one standard deviation, and (c) coefficient of variation.

or E, depending on the presence or absence of soft clay. Site specific subsurface investigation is required to determine if D or E conditions exist. In the absence of subsurface data, design response spectra should be developed for both D and E conditions and the resulting spectra enveloped." Additionally, as liquefaction and lateral spreading were documented

Table 4. Median V_{S30} values for surficial geologic units

Geologic Unit	Number of Profiles	Median V_{S30} (m/s)	NEHRP Site Class
Af	3	278	D
Qham	3	335	D
Qht2	1	346	D
Qphf	2	480	C
Qpf	8	499	C
Ppf	1	504	C
Pf*	7	564	C
Mpb	3	513	C
Lmst	1	1014	B

*TL# 12 not included in the median V_S profile for geologic unit Pf

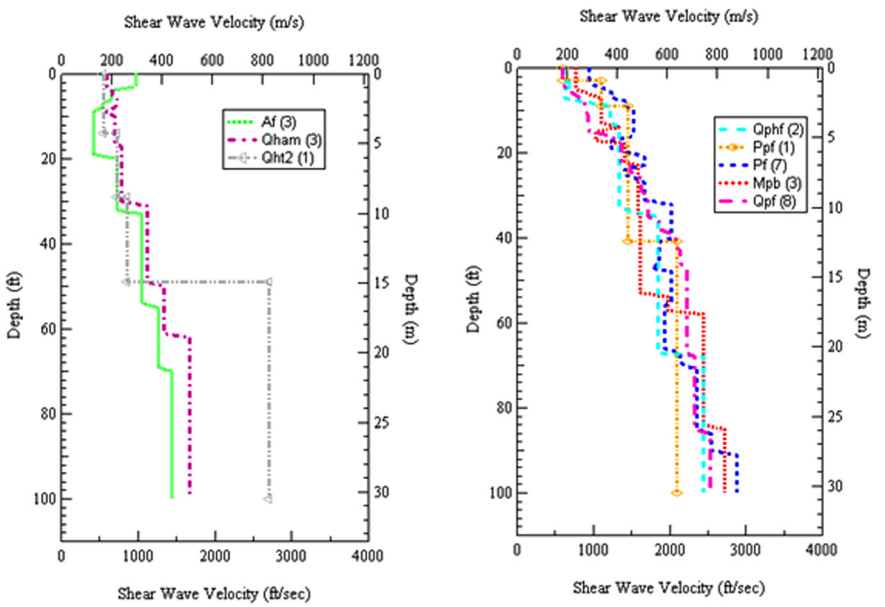

Figure 12. Median shear wave velocity profiles for: (a) Geologic units with National Earthquake Hazards Reduction Program (NEHRP) Site Class D classifications, and (b) Geologic units with NEHRP Site Class C classifications.

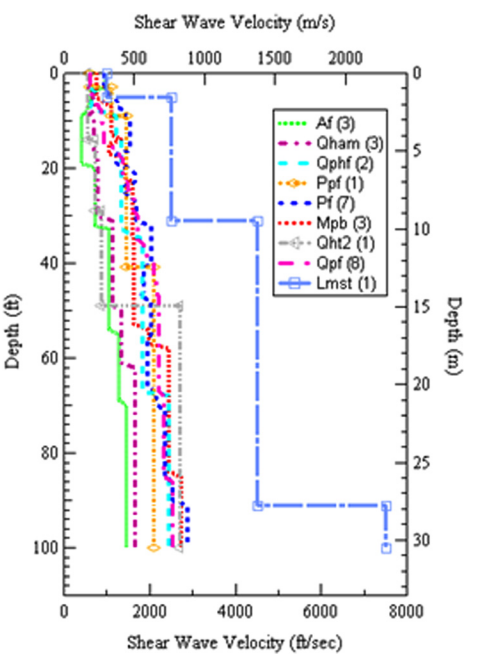

Figure 13. Median shear wave velocity profiles for all geologic units.

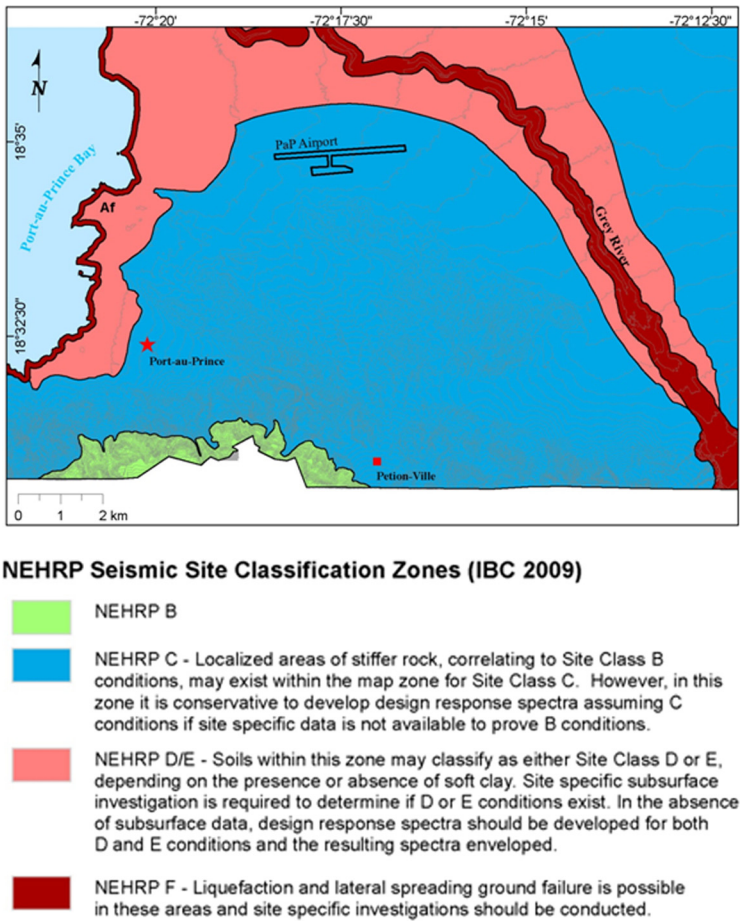

Figure 14. Shear wave velocity- and geology-based seismic site classification microzonation map for Port-au-Prince, Haiti. Note: a free geographic information system (GIS) version of this map is available from the United Nations Disaster Programme (UNDP). (Contact the lead author via e-mail for details on how to obtain it.)

following the earthquake in some artificial fill (Af) deposits along the coast and in the youngest Holocene alluvium (Qht1) along the Grey River (refer to the Geology of Port-au-Prince section), these areas have conservatively been assigned a Site Class F classification. The legend for the map reminds the user that: "Liquefaction and lateral spreading ground failure is possible in these areas and site specific investigations should be conducted." A free GIS version of the Port-au-Prince seismic site classification map is available from UNDP (please contact the lead author via e-mail for details on how to obtain it).

SUMMARY

A seismic site classification microzonation map for the greater Port-au-Prince area has been presented herein. It is based on V_S profiles obtained using the MASW method and

surficial geology defined while developing a new geologic map of the city. Free GIS versions of both the geologic map and site classification map are available from the UNDP (please contact the lead author via e-mail for details on how to obtain them).

Much of Port-au-Prince is founded on soil deposits that classify as either NEHRP Site Class C or D, based on V_{S30}. However, some areas within the mapped Holocene alluvial deposits and coastal artificial fills may classify as Site Class E or F, depending on local subsurface conditions (e.g., presence of soft clay or liquefiable soil) that cannot be determined solely with V_S profiling. Areas of the city requiring additional subsurface information for accurate site classification have been noted.

This microzonation map is a preliminary effort that can be refined as additional V_S measurements, further geologic mapping, and other information such as fundamental site period are gathered throughout the city. Furthermore, it is noted that while many microzonation efforts have been based strictly on deriving relationships between V_{S30} values and surficial geologic unit (e.g., Wills and Clahan 2006, Wong et al. 2011), more rigorous methods for seismic hazard mapping have been developed (e.g., Holzer et al. 2005, Thompson et al. 2007, Thompson et al. 2010) and may be employed as a means to enhance this work in the future. Nonetheless, this initial microzonation map is a critical step toward facilitating code-based site classification and seismic design throughout Port-au-Prince as the rebuilding process begins.

AKNOWLEDGEMENTS

This material is based on work supported by the NSF under grant numbers CMMI-1025582 and CMMI-1034828. Any opinions, findings, and conclusions or recommendations expressed in this material are those of the authors and do not necessarily reflect the views of the NSF. Additional funding for map and database development was provided by the UNDP. The authors would like to thank Mr. Yves-Fritz Joseph (Director General, Laboratoire National du Bâtiment et des Travaux Publics d'Haiti), Mr. Dieuseul Anglade (Director General, Bureau des Mines et de l'Energie, Haiti), and Mr. Jean Robert Altidor (Bureau des Mines et de l'Energie, Haiti) for their assistance in this work; Dr. Eric Calais (Purdue University and UNDP) for his efforts to facilitate training on, and implementation of our work as the rebuilding process begins; Teresa Howard (Center for Space Research at the University of Texas) for helping our team with the DEM used in this study; and the GEER steering committee for their efforts and vision to document important geotechnical issues following significant earthquakes.

REFERENCES

Assimaki, D., Li, W., Steidl, J. H., and Tsuda, K., 2008. Site amplification and attenuation via downhole array seismogram inversion: A comparative study of the 2003 Miyagi-Oki aftershock sequence, *Bulletin of the Seismological Society of America* **98**, 301–330.

Barani, S., De Ferrari, R., Ferretti, G., and Eva, C., 2008. Assessing the effectiveness of soil parameters for ground response characterization and soil classification, *Earthquake Spectra* **24**, 565–597.

Benjumea, B., Hunter, J. A., Pullan, S. E., Brooks, G. R., Pyne, M., and Alysworth, J. M., 2008. V_{S30} and fundamental site period estimates in soft sediments of the Ottawa Valley from near-

surface geophysical measurements, *Journal of Environmental and Engineering Geophysics* **13**, 313–323.

Building Seismic Safety Council (BSSC), 2003. *NEHRP Recommended Provisions for Seismic Regulations for New Buildings and Other Structures*, Federal Emergency Management Agency, Washington D.C.

Cadet, H., Bard, P. -Y., and Duval, A. -M., 2008. A new proposal for site classification based on ambient vibration measurements and the KiK-net strong motion data set, *Proceedings of the 14th World Conference on Earthquake Engineering*, 12–17 October 2008, Beijing, China.

Cassidy, J. F., and Mucciarelli, M., 2010. The importance of ground-truthing for earthquake site response, *Proceedings of the 9th U.S. National and 10th Canadian Conference on Earthquake Engineering*, 25–29 July 2010, Toronto, Canada.

Cox, B. R., and Wood, C. M., 2011. Surface wave benchmarking exercise: Methodologies, results and uncertainties, *GeoRisk2011: Risk Assessment and Management in Geoengineering*, ASCE Conf. Proc., 26–28 June 2011, Atlanta, GA (submitted).

Cox, B. R., and Wood, C. M., 2010. A comparison of linear-array surface wave methods at a soft soil site in the Mississippi Embayment, *Geo Florida2010: Advances in Analysis, Modeling & Design*, ASCE Conf. Proc., 20–24 February 2010, West Palm Beach, FL.

European Committee for Standardization (CEN), 2004. *Eurocode 8: Design of Structures for Earthquake Resistance*, *EN 1998-1*, Brussels, Belgium.

Foti, S., 2000. *Multistation Methods for Geotechnical Characterization using Surface Waves*, Ph.D. dissertation, Politecnico di Torino, Italy, 229 pp.

Foti, S., 2005. Surface wave testing for geotechnical characterization, in *Surface Waves in Geomechanics: Direct and Inverse Modelling for Soils and Rocks*, CISM Series, Number 481 (C. G. Lai and K. Wilmanski, eds.), Springer, Wien, New York, NY, 47–71.

Gallipoli, M. R., and Mucciarelli, M., 2009. Comparison of site classification from V_{S30}, V_{S10}, and HVSR in Italy, *Bulletin of the Seismological Society of America* **99**, 340–351.

Green, R. A., Olson, S. M., Cox, B. R., Rix, G., Rathje, E., Bachhuber, J., French, J., Lasley, S., and Martin, N., 2011. Geotechnical aspects of failures at Port-au-Prince Seaport during the 12 January 2010 Haiti earthquake, *Earthquake Spectra*, this issue.

Holzer, T. L., Padovani, A. C., Bennett, M. J., Noce, T. E., and Tinsley, J. C., 2005. Mapping NEHRP V_{S30} site classes, *Earthquake Spectra* **21**, 353–370.

International Code Council, Inc. (ICC), 2009. *International Building Code*, Washington D.C.

Kramer, S. L., 1996. *Geotechnical Earthquake Engineering*, Prentice-Hall, Inc., Upper Saddle River, NJ, 653 pp.

Lambert, M., Gaudin, J., and Cohen, R., 1987. *Geologic Map of Haiti, South-East Region: Port-au-Prince*, Centre d'Études et de Réalisations Cartographiques Géographiques (CERCG), National Center for Scientific Research (CNRS), Paris, France.

Olson, S. M., Green, R. A., Lasley, S., Martin, N., Cox, B. R., Rathje, E., Bachhuber, J., and French, J., 2011. Documenting liquefaction and lateral spreading triggered by the 12 January 2010 Haiti earthquake, *Earthquake Spectra*, this issue.

Park, C. B., Miller, R. D., and Xia, J., 1999. Multichannel analysis of surface waves, *Geophysics* **64**, 800–808.

Park, C. B., and Carnevale, M., 2010. Optimum MASW survey – Revisited after a decade of use, *GeoFlorida 2010: Advances in Analysis, Modeling & Design*, ASCE Conf. Proc., 20–24 February 2010, West Palm Beach, FL.

Park, D., and Hashash, Y. M. A., 2005. Evaluation of seismic site factors in the Mississippi Embayment. II. Probabilistic seismic hazard analysis with nonlinear site effects, *Soil Dynamics and Earthquake Engineering* **25**, 145–156.

Ponce, N., 1791. *Plan de la Ville des Rades et des Environs du Port-au-prince dans l'isle Saint Domingue*, Recueil de vues des lieux principaux de la colonie françoise de Saint-Domingue, Paris, France. Obtained from the John Carter Brown Library, Brown University (JCB Call Number E791 P793r / 3-SIZE).

Phung, V., Atkinson, G. M., Lau, D. T., 2006. Methodology for site classification estimation using strong-motion data from the Chi-Chi Taiwan earthquake, *Earthquake Spectra* **22**, 511–531.

Rathje, E. M., Bachhuber, J., Dulberg, R., Cox, B. R., Kottke, A., Wood, C., Green, R., Olson, S., Wells, D., Rix, G., 2011. Damage Patterns in Port-au-Prince during the 2010 Haiti earthquake, *Earthquake Spectra*, this issue.

Rathje, E., Bachhuber, J., Cox, B. R., French, J., Green, R., Olson, S., Rix, G., Wells, D., Suncar, O., 2010. *Geotechnical Engineering Reconnaissance of the 2010 Haiti Earthquake, Tech. Rep. GEER-021*, http://www.geerassociation.org/GEER_Post %20EQ%20Reports/Haiti_2010/Haiti10_index.html, published online February 2010.

Rix, G., 2005. Near-surface site characterization using surface waves, in *Surface Waves in Geomechanics: Direct and Inverse Modelling for Soils and Rocks*, CISM Series, Number 481, (C. G. Lai and K. Wilmanski, eds.), Springer, Wien, New York, NY, 1–46.

Rodriguez-Marek, A., Bray, J. D., and Abrahamson, N. A., 2001. An empirical geotechnical seismic site response procedure, *Earthquake Spectra* **17**, 65–87.

Sandikkaya, M. A., Yilmaz, M. T., Bakir, B. S., and Yilmaz, O., 2010. Site classification of Turkish national strong-motion stations, *Journal of Seismology* **14**, 543–563.

Seed, R. B., Cetin, K. O., Moss, R. E. S., Kammerer, A. M., Wu, J., Pestana, J. M., and Riemer, M. F., 2001. Recent advances in soil liquefaction engineering and seismic site response evaluation, *Proceedings, 4th International Conference on Recent Advances in Geotechnical Earthquake Engineering and Soil Dynamics*, 26–31 March 2001, San Diego, CA.

Socco, L. V., and Strobbia, C., 2004. Surface wave methods for near-surface characterisation: A tutorial, *Near Surface Geophysics* **2**, 165–185.

Sun, C. G., Kim, D. S., and Chung, C. K., 2005. Geologic site conditions and site coefficients for estimating earthquake ground motions in the inland areas of Korea, *Engineering Geology* **81**, 446–469.

Thompson, E. M., Baise, L. G., and Kayen, R. E., 2007. Spatial correlation of shear-wave velocity in the San Francisco Bay Area sediments, *Soil Dyn. Earth. Eng.* **27**, 144–152.

Thompson, E. M., Baise, L. G., Kayen, R. E., Tanaka, Y., and Tanaka, H., 2010. A geostatistical approach to mapping site response spectral amplifications, *Engineering Geology* **114**, 330–342.

Tran, K. T., and Hiltunen, D. R., 2008. A comparison of shear wave velocity profiles from SASW, MASW, and ReMi techniques, in *Proceedings of the Conference of Geotechnical Earthquake Engineering and Soil Dynamics IV, May 18–22, 2008, Sacramento, California, Geotechnical Special Publication No. 181* (CD-ROM), American Society of Civil Engineers, Reston, VA.

Wills, C. J., Clahan, K. B., 2006. Developing a map of geologically defined site-condition categories for California, *Bull. Seismol. Soc. Am.* **96**, 1483–1501.

Wong, I., Stokoe, II, K. H., Cox, B. R., Yuan, J., Knudsen, K. L., Terra, F., and Okubo, P., 2011. Shear-wave velocity characterization of the USGS Hawaiian strong motion network on

the island of Hawaii and development of a NEHRP site class map, *Bull. Seismol. Soc. Am.*, (accepted for publication).

Xia, J., Miller, R. D., Park, C. B., Hunter, J. A., Harris, J. B., and Ivanov, J., 2002. Comparing shear-wave velocity profiles inverted from multichannel surface wave with borehole measurements, *Soil Dynamics and Earthquake Engineering* **22**, 181–190.

Zaré, M., and Bard, P. Y., 2002. Soil motion dataset of Turkey: Data processing and site classification, *Soil Dynamics and Earthquake Engineering* **22**, 703–718.

Zywicki, D. J., 1999. *Advanced Signal Processing Methods Applied to Engineering Analysis of Seismic Surface Waves*, Ph.D. dissertation, Georgia Institute of Technology, Atlanta, GA, 357 pp.

Zywicki, D. J., and Rix, G. J., 2005. Mitigation of near-field effects for seismic surface wave velocity estimation with cylindrical beamformers, *J. Geotech. Geoenviron. Eng.* **131**, 970–977.

(Received 23 September 2010; accepted 10 February 2011)